Engineering Notes

Control Allocation of Solar Sail Tip Vanes with Two Degrees of Freedom

Mirue Choi* and Christopher J. Damaren†
University of Toronto, Toronto, Ontario M3H 5T6, Canada

DOI: 10.2514/1.G001703

I. Introduction

THE recent successes of IKAROS [1] and Nanosail-D2 have renewed interest in the idea of solar sailing, the method of harnessing the solar radiation pressure (SRP) via the use of large sail-like structures. IKAROS in particular has completed its mission to orbit Venus, demonstrating the solar sail's capacity for interplanetary flight. Its success has opened the door for future solar sailing missions. Since Garwin's publication in 1958 [2], researchers from a wide range of disciplines have explored topics associated with solar sailing, and attitude control is one such discipline. The wide area requirement renders commonly used attitude actuators such as reaction wheels, control moment gyros, or magnetic torquers ineffective; hence, there are several papers that introduce and develop attitude actuators that take advantage of the unique structure that solar sails possess [3–7].

In particular, the tip vane structure, as mentioned by both Wie [6] and McInnes [7], is an actuation method that uses reflective vanes located at the tips of the sail to provide the torque. Other methods that rely on the SRP (such as using gimbals or moving masses to shift the center of pressure) provide no control when the sun is not on the reflective side of the sail or if the sun is near the edge of the sail. Vanes, on the other hand, can still provide near-equal control regardless of the sun's direction because the vanes can be reoriented toward the sun.

The last statement assumes that each vane is able to reorient itself in any direction, which requires at least two rotational degrees of freedom (DOFs). However, researchers often assume that the tip vanes only possess a single degree of freedom, and the resulting loss in the control torques is simply accepted or compensated with other methods. In particular, Wie [6] shows that, for a square sail with four vanes that can rotate about the y axis, there exists a singularity where the x torque cannot be generated when the y torque is zero. In this case, a gimbaled mass is used to compensate for this loss. One of the reasons behind using a single-DOF vane over a 2-DOF vane is due to the underconstrained nature of a set of 2-DOF vanes and the resulting optimization that must be performed. For example, for a square sail with four 2-DOF vanes, the control allocation problem has eight vane angles that must be solved for, given three desired control torques and vane angle constraints. Unfortunately, the equality constraints posed by the control torques and the vane SRP force equations are highly nonlinear and cause typical numerical algorithms to fail when trying to find a solution. Torque allocation in the case of four single-DOF vanes has been considered in [8].

Instead of trying to solve the preceding problem directly, this Note proposes an alternative formulation that solves for the torques that must be produced by each vane and then solves for the vane angles from these vane torques analytically. The control allocation problem that allocates the desired torques into the vane torques is still underconstrained, but the constraints now become linear and elliptical, allowing numerical algorithms to find a global solution much more easily. The work presented here has been extended in [9], where shadowing was taken into account.

This Note is outlined as follows. Section II introduces the square sail, notations, assumptions, and the derivation of the SRP torque equation to be used in this Note. Section III introduces and defines the control allocation problem to be solved; Sec. IV shows the derivation of the elliptical constraints to be used for the problem; and Sec. V formally states the problem in a format that can be solved by a numerical algorithm. Section VI derives the analytical solution that converts the previously derived vane torques to vane angles. Finally, in Sec. VII, numerical examples that demonstrate the performance of the algorithm are presented.

II. Solar Radiation Pressure Torques Due to Two-Degree-of-Freedom Vanes

The results of this Note are based on a square solar sail, shown in Fig. 1. The body axes are as shown, with each boom aligned to the x or y axis as shown. A vane is attached at each end of the boom; hence, a total of four vanes are available for attitude control. Each vane has two rotational DOFs: for vanes 1 and 3, one along the body x axis and another along the vane y axis. For vanes 2 and 4 there is a rotation about the body y axis and a rotation about the vane x axis. For vanes 1 and 3, the y-axis rotation is denoted ϕ, and the x-axis rotation is denoted θ. Conversely, for vanes 2 and 4, the x-axis rotation is denoted by ϕ, and the y-axis rotation is denoted by θ. This convention is established assuming that each vane has the same input–output structure. Hence, from a vane frame perspective, a rotation along the x axis for vane 1 or 3 would be equivalent to a rotation along the y axis for vane 2 or 4. Also note that because of the structural symmetry, all vanes are equidistant from the geometric center when booms are assumed to be rigid. Vane frames are such that when the vane angles ϕ and θ are both zero, the vane frame is aligned with the body frame. The vane frame z axis remains aligned with the vane normal vector as ϕ and θ change.

Let $\boldsymbol{G}$ and $\boldsymbol{F}$ denote the torques and forces in Cartesian space respectively ($\boldsymbol{G}$ and $\boldsymbol{F}$ denote the corresponding components in a 3×1 column matrix). $\boldsymbol{C}$ is a 3×3 rotation matrix, $\hat{\boldsymbol{s}}$ is a unit sun vector, and $\hat{\boldsymbol{n}}$ is a unit normal vector. As well, let the subscripts b and v denote the body frame at the center of pressure of the solar sail and at the center of pressure of the vane, respectively. For convenience, assume that the center of mass, the geometric center, and the center of radiation pressure are equivalent. In addition, assume that the solar sail is ideal, that the structure remains flat and unperturbed, and that all incoming light is specularly reflected off the sail surface. These simplifications allow each vane to be represented as a point force attached at the ends of the x and y-axis booms and limit variables affecting a point force to four angles: α, β (sun angles) and ϕ, θ (vane angles). Thus, the structural dynamics of the sail and the reflective properties of the sail material are ignored.

Presented as Paper 2012-5002 at the AIAA Guidance, Navigation, and Control Conference, Minneapolis, MN, 13–16 August 2012; received 15 September 2015; revision received 21 December 2015; accepted for publication 23 December 2015; published online 28 March 2016.

*Doctoral Graduate; currently Operations Engineer, BlackBridge, Kurfürstendamm 22, 10719 Berlin, Germany.

†Professor, Institute for Aerospace Studies, 4925 Dufferin Street. Associate Fellow AIAA.

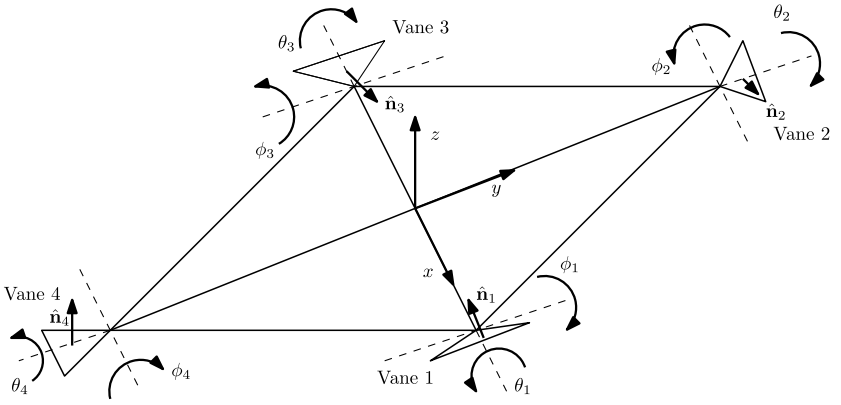

Fig. 1 2-DOF vane configurations.

As noted by McInnes in [7], the ideal force exerted on a reflective surface with sunward unit surface normal $\hat{\boldsymbol{n}}$ by a sun vector $\hat{\boldsymbol{s}}$ is

$$\boldsymbol{f}_{\text{srp}} = -2\ \text{PA}(\hat{\boldsymbol{s}}^T\hat{\boldsymbol{n}})^2\hat{\boldsymbol{n}} \tag{1}$$

where P is the SRP exerted on a reflective surface (at 1 Astronomical Unit, a constant value $4.56 \times 10^{-6}\ \text{N} \cdot \text{m}^{-2}$), and A is the total area of the reflective surface. A normalized form of the equation is given next:

$$\boldsymbol{f}_{\text{simple}} = -(\hat{\boldsymbol{s}}^T\hat{\boldsymbol{n}})^2\hat{\boldsymbol{n}} \tag{2}$$

where both the sun vector $\hat{\boldsymbol{s}}$ and the surface normal vector $\hat{\boldsymbol{n}}$ are represented in the same frame.

In a three-dimensional space, the sun vector is represented by not only the cone angle α but also by the clock angle β, as shown in Fig. 2. The sun vector in the sail body frame can then be written as

$$\hat{\boldsymbol{s}}_b = \begin{bmatrix} S_\alpha C_\beta \\ S_\alpha S_\beta \\ -C_\alpha \end{bmatrix} \tag{3}$$

where S and C represent sine and cosine functions, respectively. Vane 1 is rotated along the body x axis by θ, followed by a rotation along the rotated y axis by ϕ. The rotation matrix describing this set of rotations can be represented by the rotation matrix

$$\boldsymbol{C}_{vb} = \begin{bmatrix} C_\phi & S_\phi S_\theta & -S_\phi C_\theta \\ 0 & C_\theta & S_\theta \\ S_\phi & -C_\phi S_\theta & C_\phi C_\theta \end{bmatrix} \tag{4}$$

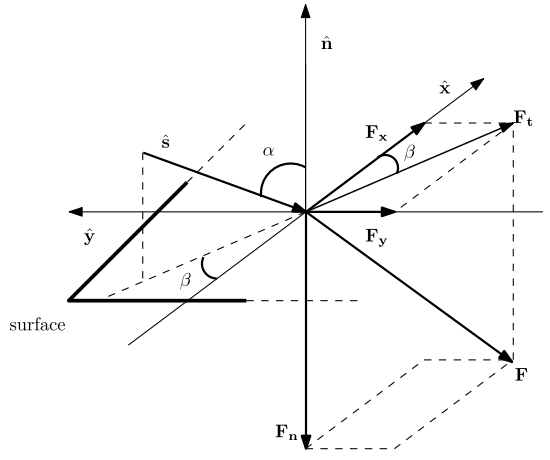

Fig. 2 Three-dimensional representation of solar radiation pressure force.

Because the vane frame is aligned with the body frame when $\phi = \theta = 0$, the sunward unit normal for each vane is $\hat{\boldsymbol{n}} = [0 \quad 0 \quad 1]^T$. Now also assume that the vane rotation does not shift the center of pressure for the SRP force, and the sail is perfectly flat along its x-y plane, with its center of pressure at the body frame origin, also on the x-y plane. Hence, it can be represented as a stationary point force attached to the end of a rigid boom. Given these assumptions, the SRP force generated by the vane in the vane frame can be written in terms of the sun angles α and β, and the vane angles ϕ and θ, as

$$\begin{aligned} \boldsymbol{f}_{v1} &= -(\hat{\boldsymbol{s}}_{vx}^T\hat{\boldsymbol{n}}_v)^2\hat{\boldsymbol{n}}_v = -((\boldsymbol{C}_{vb}\hat{\boldsymbol{s}}_b)^T\hat{\boldsymbol{n}}_v)^2\hat{\boldsymbol{n}}_v \\ &= -\begin{bmatrix} 0 \\ 0 \\ (S_\phi S_\alpha C_\beta - C_\phi S_\theta S_\alpha S_\beta - C_\phi C_\theta C_\alpha)^2 \end{bmatrix} \end{aligned} \tag{5}$$

To keep the equations simple in writing, the dot product $(\hat{\boldsymbol{s}}_{vx}^T\hat{\boldsymbol{n}}_v)$ is kept in its unexpanded form (i.e., the left side of the relationship $\hat{\boldsymbol{s}}_{vx}^T\hat{\boldsymbol{n}}_v = S_\phi S_\alpha C_\beta - C_\phi S_\theta S_\alpha S_\beta - C_\phi C_\theta C_\alpha$ is used). The force in the body frame can then be written as

$$\begin{aligned} \boldsymbol{f}_{b1} &= \boldsymbol{C}_{vb}^T\boldsymbol{f}_{v1} \\ &= \begin{bmatrix} -S_\phi \\ C_\phi S_\theta \\ -C_\phi C_\theta \end{bmatrix}(\hat{\boldsymbol{s}}_{vx}^T\hat{\boldsymbol{n}}_v)^2 \end{aligned} \tag{6}$$

Because the sail is assumed to be flat and rigid, the torque produced by this vane is simply a cross product between a vector from the origin to the vane's center of pressure and the force calculated previously, i.e.,

$$\begin{aligned} \boldsymbol{G}_{b1} &= \boldsymbol{r}_1^{\times}\boldsymbol{f}_{b1} \\ &= \begin{bmatrix} 0 \\ C_\phi C_\theta \\ C_\phi S_\theta \end{bmatrix}(\hat{\boldsymbol{s}}_{vx}^T\hat{\boldsymbol{n}}_v)^2 \end{aligned} \tag{7}$$

where the distance r_1 between the body origin and the vane center of pressure has been omitted by normalization. By following similar processes, torques produced by other vanes can also be calculated, resulting in the following vector equations:

$$\boldsymbol{G}_{b3} = \begin{bmatrix} 0 \\ -C_\phi C_\theta \\ -C_\phi S_\theta \end{bmatrix}(\hat{\boldsymbol{s}}_{vx}^T\hat{\boldsymbol{n}}_v)^2 \tag{8}$$

$$\boldsymbol{G}_{b2} = \begin{bmatrix} -C_\phi C_\theta \\ 0 \\ C_\phi S_\theta \end{bmatrix}(\hat{\boldsymbol{s}}_{vy}^T\hat{\boldsymbol{n}}_v)^2 \tag{9}$$

$$\boldsymbol{G}_{b4} = \begin{bmatrix} C_\phi C_\theta \\ 0 \\ -C_\phi S_\theta \end{bmatrix} (\hat{\boldsymbol{s}}_{vy}^T \hat{\boldsymbol{n}}_v)^2 \tag{10}$$

where, for reiteration,

$$\hat{\boldsymbol{s}}_{vx}^T \hat{\boldsymbol{n}}_v = S_\phi S_\alpha C_\beta - C_\phi S_\theta S_\alpha S_\beta - C_\phi C_\theta C_\alpha \tag{11}$$

and

$$\hat{\boldsymbol{s}}_{vy}^T \hat{\boldsymbol{n}}_v = C_\phi S_\theta S_\alpha C_\beta - S_\phi S_\alpha S_\beta - C_\phi C_\theta C_\alpha \tag{12}$$

The total control torque offered by the set of tip vanes is the combination of the four aforementioned torques and is a complex nonlinear equation of eight controllable variables. An analytical solution for the problem seems unlikely, and an attempt to solve this equation using a nonlinear solver was met with failure. An alternate method is needed to generate vane angles for a given control torque.

III. Control Allocation Problem

The goal of the control allocation problem just posed is to derive a particular set of angles that correspond to the desired torque. To this end, an optimization problem is formed as given next:

$$\begin{aligned} &\underset{\boldsymbol{\Phi}}{\text{minimize}} \ \|\boldsymbol{\Phi} - \boldsymbol{\Phi}_i\|^2 \\ &\text{subject to } \boldsymbol{G}_{b1} + \boldsymbol{G}_{b2} + \boldsymbol{G}_{b3} + \boldsymbol{G}_{b4} = \boldsymbol{G}_d \\ &-\pi < \Phi_n < \pi \end{aligned} \tag{13}$$

where $\boldsymbol{\Phi} = \text{col}\{\Phi_n\} = [\,\phi_1 \quad \theta_1 \quad \phi_2 \quad \theta_2 \quad \phi_3 \quad \theta_3 \quad \phi_4 \quad \theta_4\,]^T$, $\boldsymbol{\Phi}_i$ is the previous iteration of $\boldsymbol{\Phi}$, and $\boldsymbol{G}_d$ is the desired body frame torque vector. The cost function states that minimal changes from previous vane angle positions is desired, whereas the constraint demands that the vanes produce the desired torque. As mentioned in the previous section, this problem is challenging to solve due to its nonaffine, nonconvex nonlinear structure.

Instead of trying to solve the preceding problem, a modified problem is posed:

$$\begin{aligned} &\underset{\boldsymbol{\mathcal{G}}_b}{\text{minimize}} \ \|\boldsymbol{\mathcal{G}}_b - \boldsymbol{\mathcal{G}}_i\|^2 \\ &\text{subject to } \boldsymbol{G}_{b1} + \boldsymbol{G}_{b2} + \boldsymbol{G}_{b3} + \boldsymbol{G}_{b4} = \boldsymbol{G}_d, \\ &\text{(Satisfy Attainable Moment Set)} \end{aligned} \tag{14}$$

where $\boldsymbol{\mathcal{G}}_b$ and $\boldsymbol{\mathcal{G}}_i$ are the current and the previous vane torques in the vector form described later. Although this is not the same problem as the initial problem posed previously, it can be said to be similar, and it possesses an advantage over the first problem, which is taken advantage of to derive the proposed solution.

Because of the conditions imposed upon the sail, each vane only produces torque in two Cartesian directions, as seen in Eqs. (7–10). Hence, $\boldsymbol{\mathcal{G}}_b$ is written as

$$\boldsymbol{\mathcal{G}}_b = [\,\boldsymbol{G}_{b1y} \quad \boldsymbol{G}_{b1z} \quad \boldsymbol{G}_{b2x} \quad \boldsymbol{G}_{b2z} \quad \boldsymbol{G}_{b3y} \quad \boldsymbol{G}_{b3z} \quad \boldsymbol{G}_{b4x} \quad \boldsymbol{G}_{b4z}\,]^T \tag{15}$$

where $\boldsymbol{G}_{b1y}$ is the y component of $\boldsymbol{G}_{b1}$, and so forth. Letting these components be the controllable variables, the equality constraint is now expanded as

$$\begin{bmatrix} G_{b2x} + G_{b4x} \\ G_{b1y} + G_{b3y} \\ G_{b1z} + G_{b2z} + G_{b3z} + G_{b4z} \end{bmatrix} = \boldsymbol{G}_d \tag{16}$$

which is a linear function of $\boldsymbol{\mathcal{G}}_b$. The issue with this newly defined problem is determining the attainable moment set (AMS), or essentially defining the achievable set of torques that can be provided by each vane, and constraining the components of $\boldsymbol{\mathcal{G}}_b$ within this set.

IV. Attainable Moment Set of Vanes and Its Estimation

Visualization of the AMS can be generated by iterating through a set of values for the vane angles ϕ and θ and calculating the vane torque using the equations from the previous section, then finding the set of points that form the convex hull. The result of this procedure using Eq. (7), while assuming the vane to be reflective only on one side, is given in Fig. 3a. Although this is the AMS, it is unclear how it can be represented in an equation form so that the inequality constraint for the optimization problem defined in the previous section can be solved for. Visual inspection suggests that an ellipse would roughly fit such a shape.

Fitzgibbon et al. [10] present a direct least-square fitting method for ellipses, which would generate an equation of the ellipse that best fits a given set of points. Specifically, let the general ellipse equation for the AMS of vane 1 be written as

$$aG_{yi}^2 + bG_{yi}G_{zi} + cG_{zi}^2 + dG_{yi} + eG_{zi} + f = \boldsymbol{D}_i \boldsymbol{c} = 0 \tag{17}$$

where a through f are the ellipse constants, and

$$\begin{aligned} \boldsymbol{D}_i &= [\,G_{yi}^2 \quad G_{yi}G_{zi} \quad G_{zi}^2 \quad G_{yi} \quad G_{zi} \quad 1\,], \\ \boldsymbol{c} &= [\,a \quad b \quad c \quad d \quad e \quad f\,]^T \end{aligned} \tag{18}$$

Given a set of torque component pairs G_{yi} and G_{zi} that compose the convex hull of the AMS, the general ellipse coefficients that best fit the AMS in a least-squares sense can be calculated by solving the eigenvalue problem of the following form:

$$\boldsymbol{S}\boldsymbol{c} = \lambda \boldsymbol{C}\boldsymbol{c} \tag{19}$$

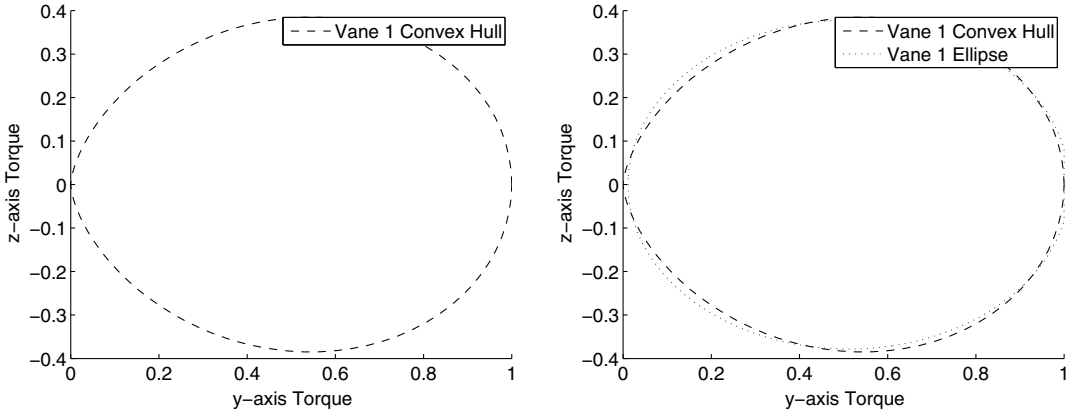

a) AMS only **b) Overlayed with an ellipse fit**

Fig. 3 AMS and its ellipse fit for vane 1 with $\alpha = 0, \beta = 0$.

where

$$\boldsymbol{S} = \boldsymbol{D}^T\boldsymbol{D}, \qquad \boldsymbol{D} = \text{col}\{\boldsymbol{D}_i\},$$

$$\boldsymbol{C} = 1\begin{bmatrix} 0 & 0 & 2 & 0 & 0 & 0 \\ 0 & -1 & 0 & 0 & 0 & 0 \\ 2 & 0 & 0 & 0 & 0 & 0 \\ 0 & 0 & 0 & 0 & 0 & 0 \\ 0 & 0 & 0 & 0 & 0 & 0 \\ 0 & 0 & 0 & 0 & 0 & 0 \end{bmatrix} \tag{20}$$

The resulting general ellipse is plotted in Fig. 3b. Although it is a reasonable approximation to the AMS, it violates the boundaries, which means the ellipse contains areas where the vane is unable to produce the specified torque. Hence, the ellipse in its current form is unsuitable as an estimation to the AMS.

To correct this discrepancy, a constrained minimization is performed on the ellipse coefficients derived by the least-squares formulation. Specifically, the goal is to find the maximum ellipse area that fits within the constraint posed by the convex hull set that describes the AMS. The area for a general ellipse can be calculated by the following equation:

$$A = \frac{2\pi h}{4ac - b^2} \tag{21}$$

where

$$h = dG_{y0} + eG_{z0} + f \tag{22}$$

and G_{y0} and G_{z0} are the x and y components of the ellipse centroid, respectively, which are calculated as follows:

$$\begin{bmatrix} G_{y0} \\ G_{z0} \end{bmatrix} = -\begin{bmatrix} 2a & b \\ b & 2c \end{bmatrix}^{-1}\begin{bmatrix} d \\ e \end{bmatrix} \tag{23}$$

The bound on the ellipse, the maximum torque set that can be produced by the vane, is represented by the following linear inequality constraint:

$$\boldsymbol{D}\boldsymbol{c} > 0 \tag{24}$$

Hence, by maximizing Eq. (21) with respect to $\boldsymbol{c}$ while satisfying the constraint Eq. (24), a generalized ellipse that is within the AMS boundary is acquired. Although the area function is nonlinear, the initial value of $\boldsymbol{c}$ calculated by solving the eigenvalue problem presented previously is sufficiently close to the desired solution that typical numerical algorithms are easily able to provide a solution. The generalized ellipse formed by one such solution is plotted in Fig. 4a, and it can be seen that this new ellipse fits tightly within the actual AMS as desired. The area ratio between the actual AMS and the ellipse estimation varies between 0.95 to 1 as the sun angles are changed.

Now, the aforementioned method may or may not be viable for on-orbit calculation as the sun angles vary with the sail orientation, but here it is assumed that it is not viable. Hence, a parameterization of the ellipse with respect to the sun angle is made using a Fourier series. Specifically, the goal is to represent the ellipse constants $\boldsymbol{c}$ in terms of a bivariate Fourier series as follows:

$$c_i(\alpha,\beta) = \chi_1 + \chi_2 S_\alpha + \chi_3 C_\alpha + \chi_4 S_\beta + \chi_5 C_\beta + \chi_6 S_\alpha S_\beta + \chi_7 S_\alpha C_\beta + \ \ldots \ = \boldsymbol{\gamma}(\alpha,\beta)\boldsymbol{\chi}_i \tag{25}$$

where c_i is one of the ellipse constants, $\boldsymbol{\gamma}(\alpha,\beta)$ is the row matrix of sinusoids, and $\boldsymbol{\chi}_i$ is the column matrix of coefficients. The maximum order of sinusoids is chosen arbitrarily; hence, the problem devolves into finding the set of coefficients for the Fourier series that best fit the set of ellipse constants for all sun angles.

This parameterization is performed as follows. First, $\boldsymbol{c}$ is calculated for a set of sun angles α and β evenly spaced between $-\pi$ and π. In parallel, $\boldsymbol{\gamma}(\alpha,\beta)$ is calculated for all of the α and β pairs. Then, each component of $\boldsymbol{c}$ and $\boldsymbol{\gamma}(\alpha,\beta)$ is stacked columnwise, and the following equation is solved for the Fourier series coefficients $\boldsymbol{\chi}_i$:

$$\Gamma\boldsymbol{\chi}_i = \boldsymbol{c}_i, \quad \boldsymbol{\Gamma} = \text{col}\{\boldsymbol{\gamma}(\alpha,\beta)\} \quad \boldsymbol{c}_i = \text{col}\{c_i(\alpha,\beta)\} \tag{26}$$

The preceding equation is solved for all six ellipse constants. Once the preceding steps are taken, generating the estimated AMS ellipse is a simple matter of calculating the ellipse constants using the Fourier series and the current sun angles. Figure 4b shows one such reconstructed ellipse using fifth-order bivariate Fourier series parameterization, overlaid on top of the original ellipse to demonstrate how well the Fourier series approximates the estimated AMS. Note that the Fourier series terms with zero or near-zero coefficients are removed to reduce storage and increase calculation speed, and after this removal procedure, only six to nine terms remain significant. The actual Fourier series terms and coefficients are given in Table 1.

The given Fourier series is specific to vane 1 only, and normally a different Fourier series would be calculated for each vane. However, after some comparison, it was found that the estimated AMS for other vanes can be derived directly from the Fourier series for vane 1. Specifically, the relationships between each vane's ellipse constant parameterizations are as follows:

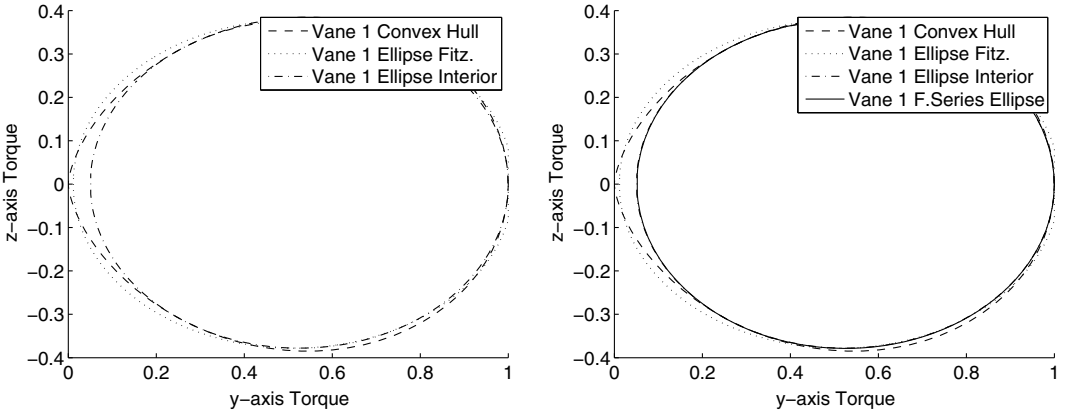

a) Overlayed with an interior ellipse fit **b) Overlayed with a fourier series ellipse fit**

Fig. 4 AMS for vane 1 with overlays for $\alpha = 0, \beta = 0$.

Table 1 Fourier series sinusoid terms and corresponding coefficients for the estimated AMS ellipse

A		*B*		*c*		*d*		*e*		*f*	
Sinusoid	Coefficient	Sinusoid	Coefficient	Sinusoid	Coefficient	Sinusoid	Coefficient	Sinusoid	Coefficient	Sinusoid	Coefficient
1	4.6252×10^{-1}	1	-6.4156×10^{-7}	1	5.1679×10^{-1}	1	-1.2271×10^{-6}	1	-1.5172×10^{-7}	1	-2.1863×10^{-4}
C_α^2	-8.6810×10^{-2}	$S_\alpha^2 S_\beta$	-2.1984×10^{-1}	C_α^2	7.6645×10^{-2}	C_α	-4.1353×10^{-1}	$S_\alpha S_\beta$	-4.2281×10^{-1}	C_α^2	2.1139×10^{-2}
C_β^2	-2.3740×10^{-2}	$S_\alpha^2 S_\beta^3$	-4.3972×10^{-3}	C_β^2	3.1945×10^{-2}	C_α^3	1.8176×10^{-2}	$S_\alpha S_\beta^3$	-2.6540×10^{-2}	C_β^2	-2.1105×10^{-2}
C_α^4	1.7733×10^{-4}	$S_\alpha^2 S_\beta^5$	-7.4852×10^{-4}	C_α^4	-2.8168×10^{-3}	C_α^5	1.0236×10^{-4}	$S_\alpha S_\beta^5$	-4.2944×10^{-4}	C_α^4	-1.6333×10^{-3}
C_β^4	-1.4713×10^{-3}	$S_\alpha^4 S_\beta$	2.9834×10^{-3}	C_β^4	8.1003×10^{-4}	$C_\alpha C_\beta^2$	-1.7289×10^{-2}	$S_\alpha^3 S_\beta$	8.4254×10^{-3}	C_β^4	-1.6435×10^{-3}
$C_\alpha^2 C_\beta^2$	2.2940×10^{-2}	$S_\alpha^4 S_\beta^3$	2.4681×10^{-3}	$C_\alpha^2 C_\beta^2$	-3.1478×10^{-2}	$C_\alpha^3 C_\beta^2$	1.7701×10^{-2}	$S_\alpha^3 S_\beta^3$	9.3914×10^{-3}	$C_\alpha^2 C_\beta^2$	2.3268×10^{-2}
$C_\alpha^2 C_\beta^4$	2.1478×10^{-3}	— —	— —	$C_\alpha^2 C_\beta^4$	3.6528×10^{-4}	$C_\alpha^3 C_\beta^4$	3.1465×10^{-4}	$S_\alpha^3 S_\beta^5$	1.6914×10^{-4}	$C_\alpha^2 C_\beta^4$	2.0365×10^{-3}
$C_\alpha^4 C_\beta^2$	9.8842×10^{-4}	— —	— —	$C_\alpha^4 C_\beta^2$	-1.9212×10^{-3}	$C_\alpha^5 C_\beta^2$	6.8806×10^{-4}	$S_\alpha^5 S_\beta$	4.4759×10^{-4}	$C_\alpha^4 C_\beta^2$	-1.9994×10^{-3}
$C_\alpha^4 C_\beta^4$	-7.3975×10^{-4}	— —	— —	— —	— —	— —	— —	$S_\alpha^5 S_\beta^3$	-3.9749×10^{-4}	$C_\alpha^4 C_\beta^4$	-6.1104×10^{-4}

$$\boldsymbol{c}_1(\alpha,\beta)=\begin{bmatrix} a(\alpha,\beta)\\ b(\alpha,\beta)\\ c(\alpha,\beta)\\ d(\alpha,\beta)\\ e(\alpha,\beta)\\ f(\alpha,\beta)\end{bmatrix},\quad \boldsymbol{c}_2(\alpha,\beta)=\begin{bmatrix} a(\alpha,\beta+\pi/2)\\ b(\alpha,\beta+\pi/2)\\ c(\alpha,\beta+\pi/2)\\ d(\alpha+\pi,\beta+\pi/2)\\ e(\alpha,\beta-\pi/2)\\ f(\alpha,\beta+\pi/2)\end{bmatrix},$$

$$\boldsymbol{c}_3(\alpha,\beta)=\begin{bmatrix} a(\alpha,\beta)\\ b(\alpha,\beta)\\ c(\alpha,\beta)\\ -d(\alpha,\beta)\\ -e(\alpha,\beta)\\ f(\alpha,\beta)\end{bmatrix},\quad \boldsymbol{c}_4(\alpha,\beta)=\begin{bmatrix} a(\alpha,\beta+\pi/2)\\ b(\alpha,\beta+\pi/2)\\ c(\alpha,\beta+\pi/2)\\ -d(\alpha+\pi,\beta+\pi/2)\\ -e(\alpha,\beta-\pi/2)\\ f(\alpha,\beta+\pi/2)\end{bmatrix} \tag{27}$$

where the functions a through f are the Fourier series parameterization of the ellipse constants. With the aforementioned, the estimated AMS for all vanes can be conveniently generated in a general ellipse equation form regardless of sun angles.

V. Formal Definition of the Control Allocation Problem

Now that an estimate to the actual AMS is available in an equation form, the optimization problem from Eq. (14) is rewritten as follows:

$$\underset{\boldsymbol{\mathcal{G}}_b}{\text{minimize}}\ \|\boldsymbol{\mathcal{G}}_b-\boldsymbol{\mathcal{G}}_i\|^2$$

$$\text{subject to}\begin{bmatrix} G_{b2x}+G_{b4x}\\ G_{b1y}+G_{b3y}\\ G_{b1z}+G_{b2z}+G_{b3z}+G_{b4z}\end{bmatrix}=\boldsymbol{G}_d,$$

$$a_iG_{biy}^2+b_iG_{biy}G_{biz}+c_iG_{biz}^2+d_iG_{biy}+e_iG_{biz}+f_i<0, i=1,3,$$

$$a_iG_{bix}^2+b_iG_{bix}G_{biz}+c_iG_{biz}^2+d_iG_{bix}+e_iG_{biz}+f_i<0, i=2,4 \tag{28}$$

Before, the constraint required that the torque values satisfy the AMS. Now, the constraint requires the torque values remain inside the general ellipse that defines the estimated AMS. The problem is now that of a quadratic cost function, three linear equality constraints, and four nonlinear inequality constraints, but more importantly every equation involved in the problem is convex. These types of optimization problems, classified as a convex optimization problem, guarantee arrival at a global optimum for any algorithm that can arrive at a local optimum and, in general, are easier to solve when using known numerical optimization algorithms [11]. For testing purpose, Matlab's fmincon function using either active-set line search or interior point methods is easily able to arrive at a solution.

There is an additional part to this problem, namely, that of determining the feasibility of the desired solution $\boldsymbol{G}_d$. Durham lists several methods to ascertain feasibility if each control variable was independently constrained [12]. This is not the case here, unfortunately. For convenience, it is assumed that if the desired solution is not achievable, a scaled solution of the desired torque while preserving directionality is desired. Letting this scalar scaling factor be λ; this problem is posed as follows:

$$\underset{\lambda,G_{zx},G_{zy}}{\text{minimize}}\ \|1-\lambda\|^2$$

$$\text{subject to } G_{zx}+G_{zy}=\lambda G_{dz},$$

$$a_k(\lambda G_k)^2+b_k\lambda G_kG_{zk}+c_kG_{zk}^2+d_k\lambda G_k+e_kG_{zk}+f_k<0,$$

$$k=x,y \tag{29}$$

where $G_{zx}=G_{b2z}+G_{b4z}$, and $G_{zy}=G_{b1z}+G_{b3z}$. The quantities a_k through f_k are the ellipse constants that define the estimated AMS boundary created by the Minkowski (geometric) sum of the estimated AMS ellipses for the pair of vanes on the same axis, and the subscript k refers to the Cartesian torque component generated by the vanes. The scaling factor λ drives the cost function to zero when it is equal to 1. This is the case where the desired torque is in fact feasible; hence, no changes are made to it when multiplied by λ. Because the goal is to constrain the desired torque to within the estimated AMS, any $\lambda > 1$ solutions would violate the ellipse constraint if the $\lambda = 1$ solution violates the constraint; hence, all cases where the desired torque is not feasible would drive the scaling factor below 1, as desired.

It should be noted that the ellipse constants used for the feasibility optimization problem are generated separately from the ellipse constants used for the actual control allocation problem. These ellipse constants are generated by combining the points that form the estimated AMS ellipse for the two vanes on the same axis in a Minkowski (geometric) sum; for example, given n points for vane 1 and m points for vane 3, the Minkowski sum of these sets of points results in nm points, where each new point is a sum of a point from vane 1 set and another point from vane 3 set. These generated points are then put through the same procedure used to generate the estimated AMS for individual vanes; a convex hull is created, which is then estimated as a generalized ellipse, whose constants are parameterized as Fourier series. The sinusoidal terms and the coefficients for this Fourier series are given in Table 2.

The preceding given numbers are valid only for the combined AMS for the x-axis vanes, but once again, there is a convenient relationship that links the combined AMS for the x-axis vanes to the combined AMS for the y-axis vanes, given next:

$$\boldsymbol{c}_y(\alpha,\beta)=\begin{bmatrix} a_y(\alpha,\beta)\\ b_y(\alpha,\beta)\\ c_y(\alpha,\beta)\\ d_y(\alpha,\beta)\\ e_y(\alpha,\beta)\\ f_y(\alpha,\beta)\end{bmatrix},\qquad \boldsymbol{c}_x(\alpha,\beta)=\begin{bmatrix} a_x(\alpha,\beta+\pi/2)\\ b_x(\alpha,\beta+\pi/2)\\ c_x(\alpha,\beta+\pi/2)\\ d_x(\alpha+\pi,\beta+\pi/2)\\ e_x(\alpha,\beta-\pi/2)\\ f_x(\alpha,\beta+\pi/2)\end{bmatrix} \tag{30}$$

Figure 5 shows the individual vane AMS, the combined AMS, and a solution set of vane torques generated by the aforementioned

Table 2 Fourier series sinusoid terms and corresponding coefficients for the combined AMS ellipse

a		*b*		*c*		*d*		*e*		*f*	
Sinusoid	Coefficient	Sinusoid	Coefficient	Sinusoid	Coefficient	Sinusoid	Coefficient	Sinusoid	Coefficient	Sinusoid	Coefficient
1	4.7975×10^{-1}	1	-6.7944×10^{-7}	1	5.3694×10^{-1}	1	-3.7380×10^{-8}	1	7.8201×10^{-10}	1	-3.4393×10^{-1}
C_α^2	-8.2014×10^{-2}	$S_\alpha^2 S_\beta$	-2.2972×10^{-1}	C_α^2	8.9863×10^{-2}	— —	— —	— —	— —	C_α^2	-1.5279×10^{-2}
C_β^2	-3.2834×10^{-2}	$S_\alpha^2 S_\beta^3$	-2.4043×10^{-3}	C_β^2	2.4907×10^{-2}	— —	— —	— —	— —	C_β^2	1.5275×10^{-2}
C_α^4	1.2695×10^{-3}	$S_\alpha^2 S_\beta^5$	-8.8293×10^{-4}	C_α^4	-1.9948×10^{-4}	— —	— —	— —	— —	C_α^4	3.1485×10^{-4}
C_β^4	-1.5202×10^{-4}	$S_\alpha^4 S_\beta$	1.8803×10^{-3}	C_β^4	1.2963×10^{-3}	— —	— —	— —	— —	C_β^4	3.0923×10^{-4}
$C_\alpha^2 C_\beta^2$	3.1941×10^{-2}	$S_\alpha^4 S_\beta^3$	1.4170×10^{-3}	$C_\alpha^2 C_\beta^2$	-2.5524×10^{-2}	— —	— —	— —	— —	$C_\alpha^2 C_\beta^2$	-1.5668×10^{-2}
$C_\alpha^2 C_\beta^4$	-2.6390×10^{-4}	$S_\alpha^4 S_\beta^5$	1.8295×10^{-4}	$C_\alpha^2 C_\beta^4$	-1.0340×10^{-3}	— —	— —	— —	— —	$C_\alpha^2 C_\beta^4$	-3.3428×10^{-4}
$C_\alpha^4 C_\beta^2$	1.5493×10^{-3}	— —	— —	$C_\alpha^4 C_\beta^2$	-2.5323×10^{-4}	— —	— —	— —	— —	$C_\alpha^4 C_\beta^2$	3.9058×10^{-4}
— —	— —	— —	— —	$C_\alpha^4 C_\beta^4$	3.8920×10^{-4}	— —	— —	— —	— —	$C_\alpha^4 C_\beta^4$	2.7415×10^{-4}

process for $\boldsymbol{G}_d = [0.5 \quad 0.3 \quad 1.3]^T$. The scaling factor is 1 (i.e., the desired torque is fully achievable), and summing up the vane torques given in the figure does indeed result in the desired torque.

VI. Analytical Solution to the Single-Vane Problem

The solution to the aforementioned control allocation problem is a set of individual, achievable torque components for each vane. The original problem, however, calls for angular parameters that control the orientation of these vanes; hence, the vane angles $\boldsymbol{\Phi}$ must still be derived from the vane torques $\boldsymbol{\mathcal{G}}_b$. Fortunately, there is an analytical solution to deriving vane angles from desired torque components when considering just one 2-DOF vane. The use of Weierstrass substitution to formulate the SRP torque turns Eqs. (7–10) into root-solving problems.

Weierstrass substitution, also known as universal trigonometric substitution, was originally developed to find integrals of trigonometric functions. Specifically, let

$$t = \tan\frac{x}{2} \tag{31}$$

Then, the following substitution can be made:

$$\sin x = \frac{2t}{1+t^2}, \qquad \cos x = \frac{1-t^2}{1+t^2} \tag{32}$$

These substitutions are valid for $-\pi < x < \pi$, which is the assumed operating range for the vanes. These substitutions are made to the SRP torque equations to rearrange them into a univariate polynomial with respect to t, which is then used to solve for the vane angle.

For example, take $\boldsymbol{G}_{b1}$ from Eq. (7). Vane angle θ can be found easily by dividing G_{bz} by G_{by} (the subscript 1 has been omitted for clarity):

$$\frac{G_{bz}}{G_{by}} = \frac{C_\phi S_\theta (\hat{\boldsymbol{s}}_v^T \hat{\boldsymbol{n}}_v)^2}{C_\phi C_\theta (\hat{\boldsymbol{s}}_v^T \hat{\boldsymbol{n}}_v)^2} = \tan\theta \tag{33}$$

Now, the only unknown is the vane angle ϕ, for which the Weierstrass substitution is used. Begin by expanding $(\hat{\boldsymbol{s}}_v^T \hat{\boldsymbol{n}}_v)^2$:

$$\begin{aligned}
(\hat{\boldsymbol{s}}_v^T \hat{\boldsymbol{n}}_v)^2 &= (S_\phi S_\alpha C_\beta - C_\phi S_\theta S_\alpha S_\beta - C_\phi C_\theta C_\alpha)^2 \\
&= S_\phi^2 S_\alpha^2 C_\beta^2 - 2S_\phi C_\phi S_\theta S_\alpha^2 S_\beta C_\beta - 2S_\phi C_\phi C_\theta S_\alpha C_\alpha C_\beta + C_\phi^2 S_\theta^2 S_\alpha^2 S_\beta^2 \\
&\quad + 2C_\phi^2 S_\theta C_\theta S_\alpha C_\alpha S_\beta + C_\phi^2 C_\theta^2 C_\alpha^2 \\
&= aS_\phi^2 + bS_\phi C_\phi + cC_\phi^2, \\
a &= S_\alpha^2 C_\beta^2, \\
b &= -2(S_\theta S_\alpha^2 S_\beta S_\beta + C_\theta S_\alpha C_\alpha C_\beta), \\
c &= S_\theta^2 S_\alpha^2 S_\beta^2 + 2S_\theta C_\theta S_\alpha C_\alpha S_\beta + C_\theta^2 C_\alpha^2
\end{aligned} \tag{34}$$

where constants a, b, and c were defined for conciseness. The preceding expression can be substituted into either the expression for G_{by} or G_{bz}. For demonstration purposes, G_{by} is used here. Assuming $t = \tan\frac{\phi}{2}$ and making the appropriate substitutions to S_ϕ and C_ϕ,

$$\begin{aligned}
G_{by} &= C_\phi C_\theta (\hat{\boldsymbol{s}}_v^T \hat{\boldsymbol{n}}_v)^2 \\
&= C_\phi C_\theta (aS_\phi^2 + bS_\phi C_\phi + cC_\phi^2) \\
&= \frac{1-t^2}{1+t^2} C_\theta \left[a\left(\frac{2t}{1-t^2}\right)^2 + b\left(\frac{2t}{1-t^2}\right)\left(\frac{1-t^2}{1+t^2}\right) + c\left(\frac{1-t^2}{1+t^2}\right)^2 \right]
\end{aligned} \tag{35}$$

Expanding and rearranging the preceding equation gives

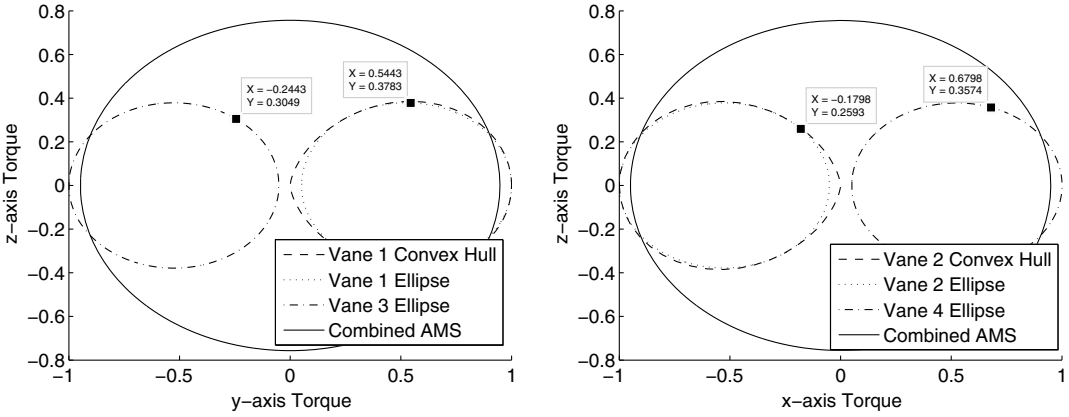

a) Vanes 1 and 3 **b) Vanes 2 and 4**

Fig. 5 Estimated AMS and the results of the algorithm for $\boldsymbol{G}_d = [0.5 \quad 0.3 \quad 1.3]^T$ with $\alpha = 0, \beta = 0$.

$$(G_{by}+cC_\theta)t^6+(-2bC_\theta)t^5+[3G_{by}-(3c-4a)C_\theta]t^4 + (4bC_\theta)t^3+[3G_{by}-(4a-3c)C_\theta]t^2+(-2bC_\theta)t+(G_{by}-cC_\theta)=0 \quad (36)$$

Because the preceding is a univariate algebraic equation, its roots can be solved for using common root-solving techniques. The vane angle ϕ can then be derived from t by using the definition of Weierstrass substitution (i.e., $t = \tan(\phi/2)$). The polynomial is of sixth order; hence, up to six solutions exist for t. Neglecting any imaginary solutions, the remaining roots and the resulting vane angles are then substituted back into Eq. (7) to produce the vane torques. The vane angles that produce the correct vane torques and are closest to the previous vane angles are chosen as the true solution.

The preceding steps are repeated in a similar fashion for all vanes. For vane 2, Eq. (9) is used to derive the equations for the vane angles. The equation for deriving θ_2 can be written as

$$\frac{-G_{b2z}}{G_{b2x}} = \tan\theta_2 \quad (37)$$

whereas the algebraic polynomial for ϕ_2 is written as

$$(G_{b2x}-cC_{\theta 2})t^6+(2bC_{\theta 2})t^5+[3G_{b2x}+(3c-4a)C_{\theta 2}]t^4+(-4bC_\theta)t^3 + [3G_{b2x}+(4a-3c)C_{\theta 2}]t^2+(2bC_{\theta 2})t+(G_{b2x}+cC_{\theta 2})=0 \quad (38)$$

where

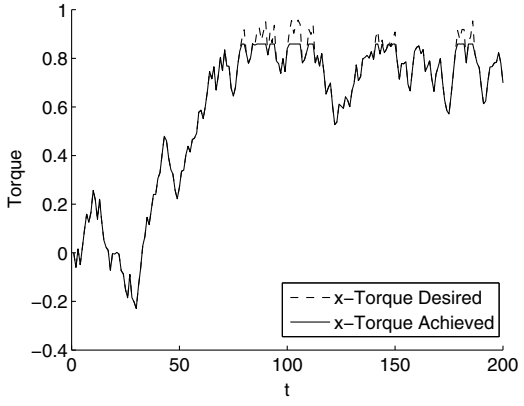

a) Desired (dashed) and achieved (solid) torques (x-axis)

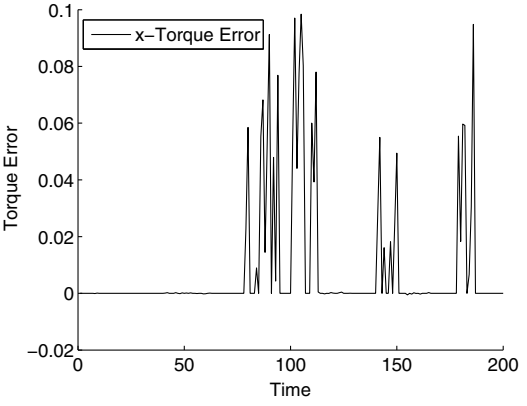

b) Error between desired and achieved torques (x-axis)

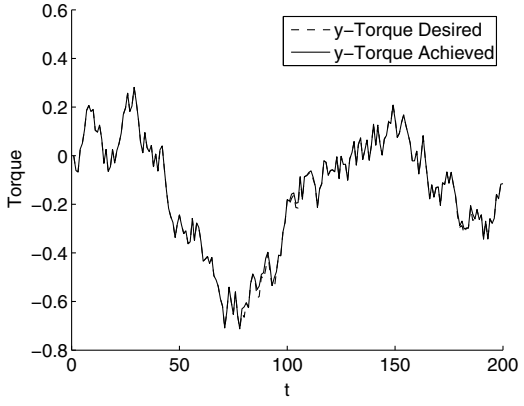

c) Desired (dashed) and Achieved (solid) Torques (y-axis)

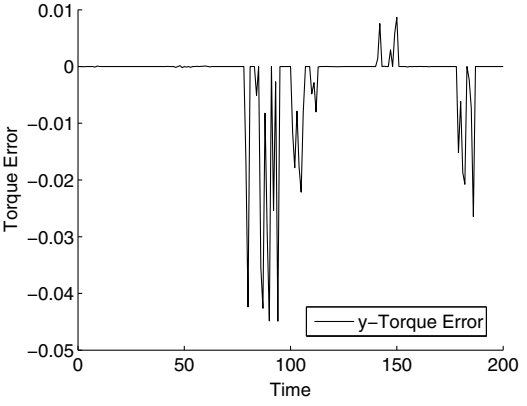

d) Error between desired and achieved torques (y-axis)

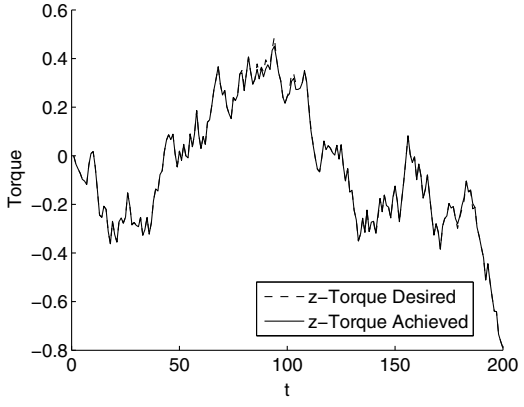

e) Desired (dashed) and achieved (solid) torques (z-axis)

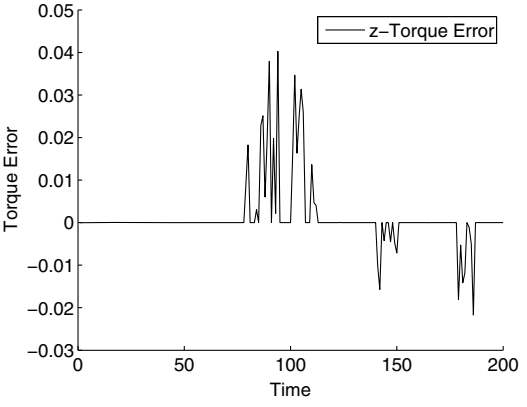

f) Error between desired and achieved torques (z-axis)

Fig. 6 Simulation results with $\alpha = \pi/4, \beta = \pi/3$.

$$a = S_\alpha^2 S_\beta^2, \qquad b = 2(C_{\theta 2} S_\alpha C_\alpha S_\beta - S_{\theta 2} S_\alpha^2 S_\beta C_\beta)$$
$$c = S_{\theta 2}^2 S_\alpha^2 C_\beta^2 - 2 S_{\theta 2} C_{\theta 2} S_\alpha C_\alpha C_\beta + C_{\theta 2}^2 C_\alpha^2 \tag{39}$$

The roots of the polynomial can be solved for and ϕ_2 derived from the roots via Weierstrass substitution as before.

For vane 3, the same algorithm used to calculate the angles for vane 1 can be used, by noting that the right-hand side of Eq. (8) is simply the sign-inverted right-hand side of Eq. (7). Vane angle θ_3 is calculated the same, whereas vane angle ϕ_3 is calculated by running through the same process for ϕ_1 while using $-G_{b3y}$ in place of G_{b1y}, to reflect the difference in sign. A similar process applies for vane 4, except it uses the algorithm for vane 2 instead of vane 1.

VII. Numerical Example

The capacity of the solution implemented in Matlab is demonstrated by using a randomly generated set of desired torques and using the preceding algorithm to calculate a set of vane angles that would correspond to it. Specifically, a torque value is generated by using the following equation:

$$\boldsymbol{G}_{d,k} = \boldsymbol{G}_{a,k-1} + \texttt{rand}_3(0.1) \tag{40}$$

where $\boldsymbol{G}_{d,k}$ is the current desired torque, $\boldsymbol{G}_{a,k-1}$ is the previously achieved torque, and $\texttt{rand}_3(0.1)$ generates a 3×1 vector containing random component values between -0.1 and 0.1. The number 0.1 is chosen to facilitate gradual traversal of the range of achievable normalized torques. The previously achieved torque is used in place of previously desired torque to prevent the desired torques from building up to unreasonably high values. A total of 200 desired torques and the corresponding vane angles are generated, where the number 200 is chosen based on the observation that there is sufficient variance in the desired torques by then to demonstrate the performance of the algorithm. For the minimization process, fmincon offers a number of optimization algorithms. After test simulations, it was determined that the active-set line search method works best and is used for this simulation.

Figures 6 and 7 are a set of plots describing the results of the simulation for $\alpha = \pi/4$, $\beta = \pi/3$. Figures 6a and 6c, 6e show the desired torques as well as the torques achieved from the vane angles generated using the control allocation process, one plot per axis. The actual error between the desired and the achieved torques is given in Figs. 6b, 6d, and 6f, and a few spikes of error can be seen. This error is actually caused by the desired torque exceeding the achievable torque and is a behavior that is desired. This shows that the feasibility analysis is correctly performing its job and restricting the given desired torque to within the feasibility bound.

The vane torques are given in Figs. 7a and 7b, along with each vane's estimated AMS, and the vane angles are given in Fig. 7c. It can be seen that the vane torques are constrained strictly within the estimated AMS, and the cost function that minimizes the changes in individual vane torques also has an effect on the vane angles, which changes gradually instead of spiking from one value to another as the desired torque changes.

The processing speed for the algorithm is measured by the number of iterations taken by the fmincon function to arrive at a solution, which is shown in Fig. 7d. It can be seen that, for both the feasibility analysis and the control allocation, the number of iterations to arrive at a solution remains small. There is a notable spike in the solution around the middle, but this is a boundary case, as Fig. 6d and its location of the error spike shows. Actual computing time for the entire simulation on a modern personal computer was measured to be around 20 s, which included continuous updates to the plots given previously.

It is worth noting that, although this simulation demonstrates the capability of the control allocation scheme under ideal conditions, it does not make any attempt to account for issues such as optical

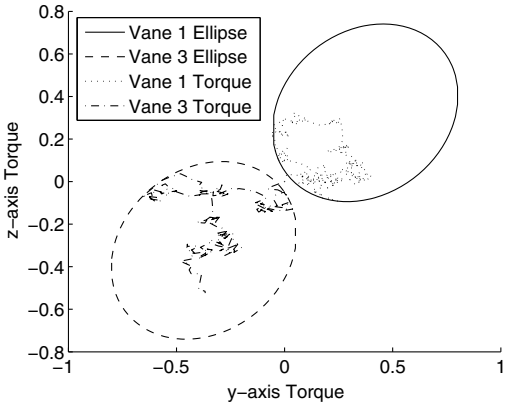

a) Vane torques for vanes 1 and 3 (lines within ellipse)

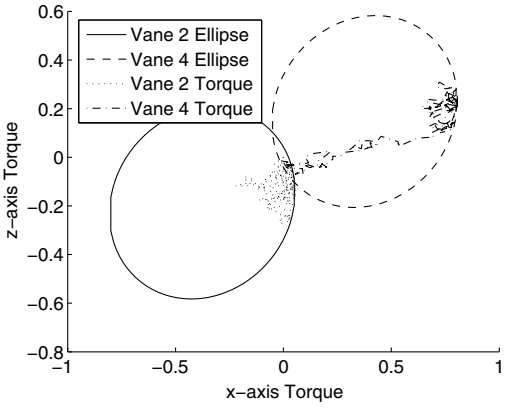

b) Vane torques for vanes 2 and 4 (lines within ellipse)

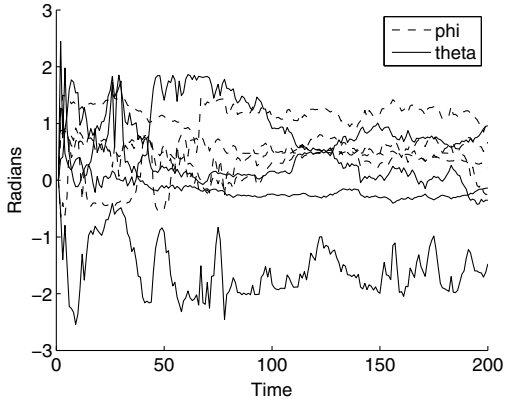

c) Vane angles

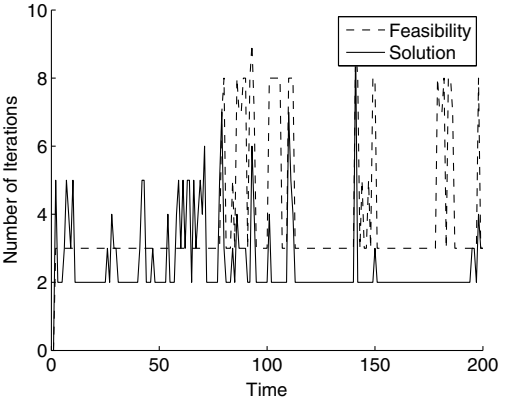

d) Fmincon iteration counts

Fig. 7 Simulation results with $\alpha = \pi/4, \beta = \pi/3$ (continued).

nonideality of the reflective surface or the flexibility of the booms to which the vanes are attached.

VIII. Conclusions

A method for solving the control allocation problem posed by four 2-DOF vanes on a square solar sail was presented. Numerical examples were provided that demonstrated the feasibility of the algorithm. The algorithm presented in this Note is not complete because there are other factors that must be taken into account. One such factor is the nonlinearity of the reflective surface of the vane, which would change the shape of the attainable moment set (AMS) and render the analytic solution to the single-vane problem invalid. The change in AMS will be static and hence can be accounted for from the ground-testing phase. Another factor is the structural dynamics of the booms to which the vanes are attached, which would render the AMS time-dependent. This is a critical issue that could render the derived solution useless because the AMS will need to be recalculated on the fly or the initial derivation of the estimated AMS will somehow need to include the structural dynamics factor.

References

[1] Tsuda, Y., Mori, O., Funase, R., Sawada, H., Yamamoto, T., Saiki, T., Endo, T., and Kawaguchi, J., "Flight Status of IKAROS Deep Space Solar Sail Demonstrator," *Acta Astronautica*, Vol. 69, Nos. 9–10, 2011, pp. 833–840. doi:10.1016/j.actaastro.2011.06.005

[2] Garwin, R. L., "Solar Sailing—A Practical Method of Propulsion Within the Solar System," *Jet Propulsion*, Vol. 28, No. 3, 1958, pp. 188–190.

[3] Stuck, B., "Solar Pressure Three-Axis Attitude Control," *Journal of Guidance, Control, and Dynamics*, Vol. 3, No. 2, 1980, pp. 132–139. doi: 10.2514/3.55960

[4] Bolle, A., and Circi, C., "Solar Sail Attitude Control Through In-Plane Moving Masses," *Proceedings of the Institution of Mechanical Engineers, Part G: Journal of Aerospace Engineering*, Vol. 222, No. 1, 2008, pp. 81–94. doi:10.1243/09544100jaero223

[5] Wie, B., "Solar Sail Attitude Control and Dynamics, Part 1," *Journal of Guidance, Control, and Dynamics*, Vol. 27, No. 4, 2004, pp. 526–535. doi:10.2514/1.11134

[6] Wie, B., "Solar Sail Attitude Control and Dynamics, Part 2," *Journal of Guidance, Control, and Dynamics*, Vol. 27, No. 4, 2004, pp. 536–544. doi:10.2514/1.11133

[7] McInnes, C., *Solar Sailing: Technology, Dynamics and Mission Applications*, Springer, Praxis, 1999, Chap. 2. doi:10.1007/978-1-4471-3992-8

[8] Metler, E., Açikmeşe, A. B., and Ploen, S. R., "Attitude Dynamics and Control of Solar Sails with Articulated Vanes," *AIAA Guidance, Navigation, and Control Conf. and Exhibit*, AIAA Paper 2005-6081, Aug. 2005, doi: 10.2514/6.2005-6081

[9] Kun, Z., "Control Capability and Allocation of Solar Sail Tip Vanes over Bounded Movement," *Journal of Guidance, Control, and Dynamics*, Vol. 38, No. 7, 2015, pp. 1340–1344. doi:10.2514/1.G000938

[10] Fitzgibbon, A., Pilu, M., and Fisher, R., "Direct Least Square Fitting of Ellipses," *IEEE Transactions on Pattern Analysis and Machine Intelligence*, Vol. 21, No. 5, 1999, pp. 476–480. doi:10.1109/34.765658

[11] Boyd, S., and Vanderberghe, L., *Convex Optimization*, Cambridge Univ. Press, Cambridge, England, U.K., 2009, Chap. 4. doi: 10.1017/cbo9780511804441

[12] Durham, W. C., "Constrained Control Allocation," *Journal of Guidance, Control, and Dynamics*, Vol. 16, No. 4, 1993, pp. 717–725. doi:10.2514/3.21072